SHORT COMMUNICATION

The Mechanism of Proton Exclusion in Aquaporin Channels

Boaz Ilan,[1] **Emad Tajkhorshid,**[2] **Klaus Schulten,**[2] **and Gregory A. Voth**[1,*]

[1]*Department of Chemistry and Henry Eyring Center for Theoretical Chemistry, University of Utah, Salt Lake City, Utah 84112-0850*

[2]*Theoretical and Computational Biophysics Group, Beckman Institute, University of Illinois at Urbana-Champaign, Urbana, Illinois 61801*

Abstract: **The mechanism of proton exclusion in aquaporin channels is elucidated through free energy calculations of the pathway of proton transport. The second generation multistate empirical valence bond (MS-EVB2) model was applied to simulate the interaction of an excess proton with the channel environment. Jarzynski's equality was employed for rapid convergence of the free energy profile. A barrier sufficiently high to block proton transport is located near the channel center at the NPA motif—a site involved in bi-orientational ordering of the embedded water-wire in absence of the excess proton. A second and lower barrier is observed at the selectivity filter near the periplasmic outlet where the channel is narrowest. This secondary barrier may be essential in filtering other large solutes and cations. Proteins 2004;55:223–228.** © 2004 Wiley-Liss, Inc.

Key words: proton transport; multistate empirical valence bond; aquaporin channels

INTRODUCTION

Rapid water conduction is essential for certain physiological processes such as reabsorbtion of water into blood and production of saliva and tears. A family of membrane protein channels, the aquaporins,[1–3] has evolved to facilitate osmotic and concentration driven water conduction at a rate about 10–20-fold larger than permeation through protein-free lipid bilayers.[2] Aquaporins are selective at physiological conditions, allowing water permeation while excluding charged solutes,[3] including protons, and thereby preserve electrochemical potentials across cell membranes. This enables, for example, regulation of water conduction in plant roots, in response to flooding, by cytosolic pH.[4] In this article we study proton transport (PT) through the *Escherichia coli* glycerol facilitator (GlpF), a member of the aquaglyceroporins subfamily, which conduct both water and linear polyalchohols such as glycerol.

The accumulated evidence[5] suggests that protons propagate through water filled protein channels, as through bulk water, by a Grotthuss-type mechanism.[6] This mechanism involves successive proton "hops" between adjacent water molecules. The hop step consists of a simultaneous conversion of a covalent bond into a hydrogen bond in one water molecule and the corresponding formation of a covalent bond in a nearby water molecule. Confinement by narrow pores reduces the dimensionality of the hopping process and constrains the orientational freedom of water molecules, implicit through the Grotthuss mechanism. The process of PT was recently simulated[7] in a hydrophobic channel modeled by a repulsive potential.[8] The proton mobility was found to increase 10-fold with decreasing pore radius. This enhancement was ascribed to the formation of a 1D "water wire" as the pore radius was decreased to 2 Å. Although estimates vary,[5] proton conduction through the gramicidin ion channel seems not much different from that in bulk water.

A 2.2 Å resolution X-ray structure of GlpF has resolved[9] a homotetrameric structure with each monomeric unit spanning an hourglass shaped trans-membrane aqueous pore. Figure 1 depicts a single monomer. Each monomeric channel is composed of two half-membrane spanning repeats, and about half of each repeat is α-helical. The N-termini of the helical repeats meet at the Asn-Pro-Ala (NPA) motifs located near the channel center (blue residues in Fig. 1); the NPA motif is conserved among all the aquaporin proteins. MD simulations of water transport in aquaporins[10,11] depicted single-file diffusion along the curvilinear constriction region with water flux rates in agreement with experiment. These studies proposed that the NPA motif[11] and selectivity filter[10] may be the principal factors in the mechanism of proton exclusion.
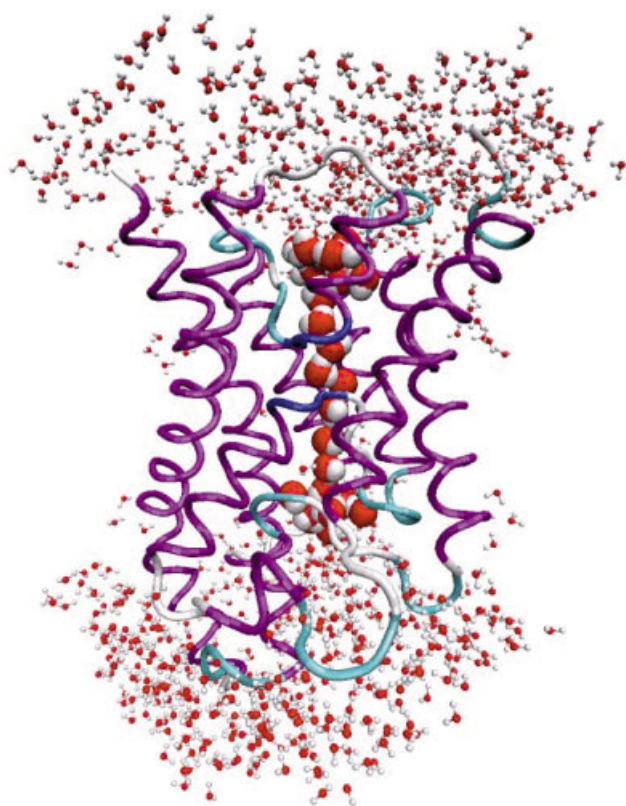
Fig. 1. Schematic view of a single GlpF monomer. Blue sections correspond to Asn-Pro-Ala residues of the NPA motifs, and the cytoplasmic end is at the top. The α-helical section of the backbone is colored purple. Water molecules are enlarged in the constriction region and the reverse orientation occurs at the NPA motif. The image was created with VMD software.
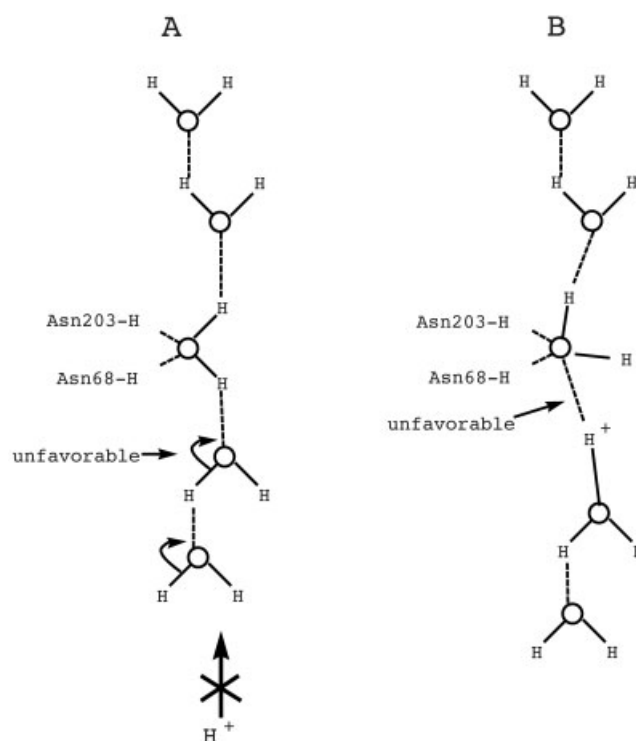

Fig. 2. The mechanism of proton exclusion (adapted from Fig. 3 of Ref. 11). An excess proton attempting to permeate the channel (A) would have to work against the intrinsic (in its absence) bi-orientation of the water-file, as induced by the electrostatic fields[11] of the protein matrix. Approaching the NPA motif (B) the excess proton would face prohibitive energetics.

The amido groups (NH_2) of Asn 203 and Asn 68 of the NPA motifs extend into the constriction region [Fig. 2(A)], forming hydrogen bonds with an oxygen atom of a water molecule, and thereby compelling its dipole moment to orient perpendicular to the channel axis. The orientation of this water molecule is further stabilized by the presence of hydrophobic residues above and below along the constriction pore. The two neighboring water molecules face this water molecule with their oxygen atoms, ordering the rest of the water molecules on either side, and aligning their hydrogens away from the channel center. A proton attempting to permeate the channel will presumably confront an already fully coordinated water molecule at the NPA motif [Fig. 2(B)].

In contrast, a nonprotonated water-wire inside the proton-conducting gramicidin channel exhibits uniform orientation (transient with equal probability in either direction). The selectivity filter in GlpF, for which the pore radius is smaller than 3.5 Å, further inhibits PT. Disruptions in hydrogen bond connectivity between successive water molecules residing in the selectivity filter were also observed in Ref. 10. These hypotheses are, however, conjectures based on hydrogen bonding patterns, and they must be validated by studies that incorporate an explicit simulation of the proton transport.

A methodology to explicitly simulate PT in MD simulations has been developed over a number of years in the Voth group.[12–18] This approach can accurately describe excess protons, including the Grotthuss mechanism, in aqueous[12–15] and biological[16–18] environments. For a discussion of the relationship between this approach and other attempts to simulate explicit proton transport, see Ref. 13. The current version, MS-EVB2, has been optimized and refined to reproduce the key features of PT from both experiment and ab initio MD,[19] e.g., geometries and energetics of protonated clusters, proton hopping rate, spectroscopy and density of vibrational states, and relative stabilities of Eigen, $H_9O_4^+$, and Zundel, $H_5O_2^+$, cations in bulk water. The combination of the MS-EVB2 model with Jarzynski's free energy method[20–22] thus enables the calculation of the potential of mean force (PMF) for PT along reaction coordinates of biological systems, such as the aquaporin and gramicidin channels.

METHODS

MS-EVB2 model

At each MD time step, the relevant "valence bond" states corresponding to different possible associations of an excess proton with water molecules within several solvation shells are considered.[12,13] Figure 3(A,B) presents a schematic snapshot of solvated proton configurations, characteristic of the Zundel, $H_5O_2^+$, and Eigen, $H_9O_4^+$, cations,
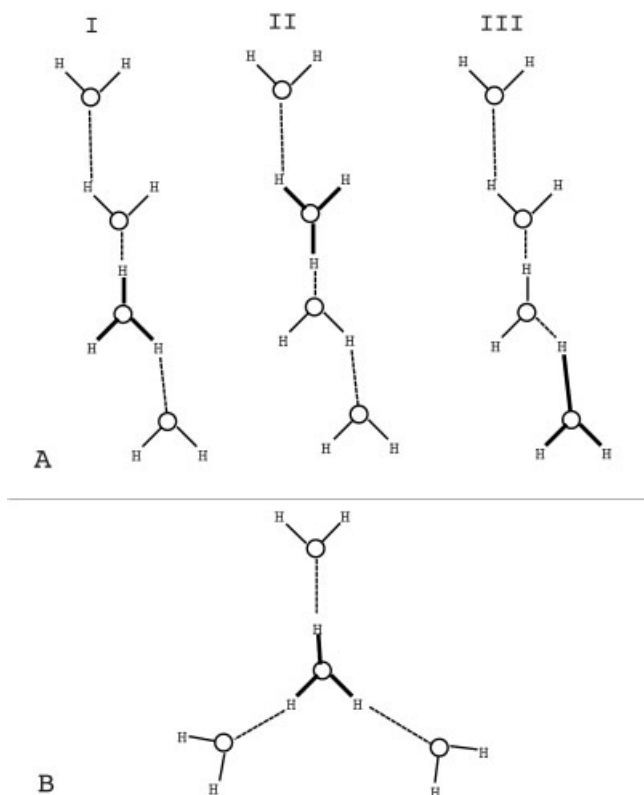
Fig. 3. The schematic configuration in (A) is characteristic of the Zundel, $H_5O_2^+$, cation. Three different MS-EVB2 states, I, II, and III may be identified. Solid and dotted lines represent covalent and hydrogen bonds, respectively. The thick solid lines represent a hydronium ion. In representative Zundel configurations two states would have equal weights of ~0.5; for this configuration (A) these would be states I and II. The hydronium state in the schematic configuration B, is characteristic of an Eigen cation, $H_9O_4^+$, with an amplitude of ~0.65.

respectively. Three possible states I, II, and III are identified in Figure 3(A). Each state in this simplified example consists of a hydronium ion and 3 water molecules. The number of states, N, may vary with time, and PT occurs by continuous, deterministic transitions between these states. An empirical valence bond method is used to construct an $(N \times N)$ Hamiltonian matrix, $\hat{H}$. The ground state potential energy, E_0, and eigenvector, $\tilde{c}$, are obtained by solving $\tilde{c}^T \hat{H} \tilde{c} = E_0$ for each nuclear configuration and forces for the MD integrator are then generated via the Hellmann Feynman Theorem. Assuming the weights of states I and II, c_I^2 and c_{II}^2, respectively, are ~0.5, the configuration in Figure 3(A) would be representative of the Zundel cation.

The Zundel cation is more prevalent than the Eigen cation in channel embedded water-wires.[7,18] The latter cation, which is more hydronium-like and slightly more stable than the Zundel in bulk water,[12] usually has an amplitude $c_1^2 \approx 0.65$ [Fig. 3(B)] with the second largest amplitude being $c_2^2 \approx 0.1$. (Note that in the present work the explicit binding of the proton with protein residues is not considered). Because of the delocalized nature of the excess proton, its position must be identified[7] with the center of excess charge (CEC):

$$\boldsymbol{r}_{cec}(t) = \sum_{i=1}^{N} c_i^2 \boldsymbol{r}_i(t), \tag{1}$$

where $\boldsymbol{r}_i(t)$ are center of charge vector of hydronium in the ith MS-EVB2 state at time t.

Simulation model

We have adopted a reduced model (Fig. 1) represented by a single monomer with 5 Å water shells on either side. The starting configuration was taken from a snapshot[11] saved after 3 ns of equilibrium MD simulation of the membrane-embedded tetramer. The subgroup of α-carbon backbone atoms whose distances to all the water molecules in the constriction region are all greater than 10 Å were harmonically tethered during the simulation to their initial positions. The tethering force constants we chose, 10 kJ/(mole Å^2), reproduce RMSD of relatively rigid protein channels,[18] and the absence of tethering along the proton conduction pathway allows for minor structural reorganization due to its presence. The tethering procedure is justified on ground of the rigidity imparted by the neighboring protein channels on each other. The water molecules at the caps were not confined. A total of 6329 atoms including an excess proton and two Cl$^-$ atoms for total neutrality were included in the simulation. The Cl$^-$ anions were not observed to enter the constriction region. Simulations were carried with the DL_POLY MD package[23] modified to include the MS-EVB2 algorithm. An NVT ensemble was maintained by a Nose-Hoover thermostat with a relaxation constant of 0.2 ps; the temperature was set to be T = 308 K. The electrostatics were calculated with the Ewald method, and the cutoff radii for Lennard-Jones and real-space Coulombic interactions were 9 and 10 Å, respectively. The MD time step was 1 fs, and the protein interactions were modeled by the AMBER force field[24] with water represented by the flexible TIP3P model.[25] The approximation associated with the reduced model is justified because the immediate channel environment is the most relevant for the transport properties of the excess proton. Support to this assumption can be drawn from MD simulations,[26] which show that the electrostatic field along the water conduction pathway is barely influenced by the long-range electrostatic contributions from the embedding membrane and neighboring channels.

Potential of mean force calculations

Jarzynski's equality[20,21] was used in this work to calculate the PMF of PT through the aquaporin channel. This equality states

$$e^{-\beta \Delta F} = \langle e^{-\beta W} \rangle, \tag{2}$$

where ΔF corresponds to the free energy difference between two parameterized states $\lambda(0)$ and $\lambda(t)$, and W stands for the nonequilibrium work performed along irreversible paths connecting these states, with $\beta = 1/(k_B T)$. The average is carried out beginning with an equilibrium ensemble of initial conditions consistent with $\lambda(0)$. We "pull" the proton CEC [Eq. (1)] along the z-axis by tether-

TABLE I. The Average Work Values (kcal/mol) for Pulling an Excess Proton in Bulk Water a Distance of 1 Å Forward and Backward along the z-axis in the Presence of an Electric Field in the z-direction of 10 kcal/(mol · Å · e)[†]

Speed (Å/ns)	1	5	10	25
Forward	−9.847	−9.252	−8.526	−6.189
Backward	10.145	10.740	11.541	13.612
"Cyclic" dissipative work	0.008	0.008	−0.067	0.199

[†]Subtracting the dissipative work accumulated in the forward direction from that accumulated in the backward direction gives values close to zero at all speeds (third row). Standard deviations (not included) increase with pulling speed.

ing the z-coordinate of the CEC, z_{cec}, to a steadily moving coordinate, $\lambda(t) = (0, 0, \lambda_0 + v \cdot t)$, according[22,27] to $u(z_{cec}, t) = (k/2)(z_{cec} - \lambda_0 - v \cdot t)^2$. The z-axis is also the channel axis except for small curvilinear detours; k is the spring constant, t is time, v is the constant pulling velocity, and λ_0 is a constant. The z_{cec} dependence on time is implicit. Jarzynski's equality holds at any given pulling speed. The work along paths connecting $z = \lambda_0$ with $z = \lambda_0 + v \cdot t$ is given by

$$W = \int_0^t \frac{\partial u(z_{cec}, t')}{\partial t'} \, dt'. \quad (3)$$

In the limit $t \rightarrow \infty$, W is reversible and equals ΔF. Within the stiff spring approximation, W is given by $-vk \int_0^t (z_{cec} - \lambda_0 - t' \cdot v)dt'$ and z_{cec} can be identified with λ. In this work 20 forward pulling trajectories were carried out from $z = -15$ Å to $z = 15$ Å at $v = 20$ Å/ns and $k = 2780$ pN/Å. Different initial conditions were generated by initiating pulling at varying times after an equilibration period with the proton tethered at $z = -15$ Å. Similarly 10 backward pulling trajectories were carried out from $z = 15$ Å to $z = -15$ Å at the same rate and spring constant. The backward and forward PMFs were then calculated separately according to Eq. (2). One criteria for the convergence of Eq. (2) is the appearance of good agreement between the backward and forward PMFs. Accelerated convergence can also be achieved by averaging the backward and forward PMFs so that the dissipative work accumulated in each direction is approximately canceled out. No systematic errors are introduced through this averaging procedure since Jarzynski's equality holds separately whether the proton is pulled forward or backward. A similar approach based on information from both forward and backward work functions is discussed in Ref. 28. According to the Second Law of Thermodynamics, the thermodynamic dissipative work is always non-negative, $\langle W \rangle - \Delta F \geq 0$; yet, in principal, work functions of individual trajectories may be smaller than ΔF.

As a test case for this "cyclic" averaging procedure an excess proton in 19 water molecules was pulled at varying speeds forward and backward along the z-axis in the presence of a uniform electric field along the z-direction of 10 kcal/(mole · Å · e). Results from these test calculations are presented in Table I. From left to right, with increasing
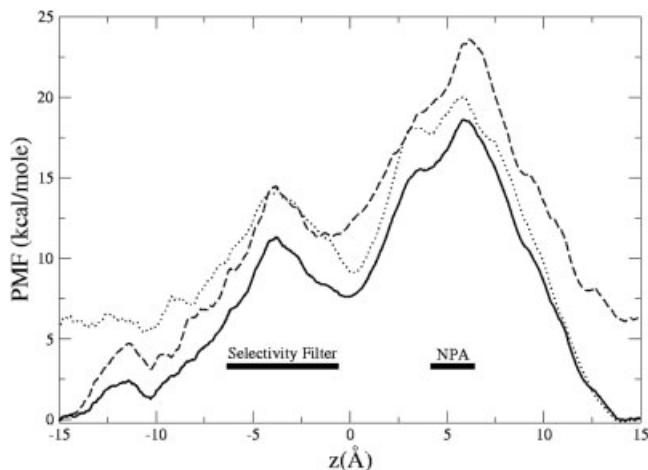

Fig. 4. PMF of PT along the z-axis of the GlpF protein channel. Dashed and dotted lines correspond to forward and backward pulling profiles, respectively. Solid line is the average of the forward and backward profiles, shifted to equal zero at $z = -15$ Å. The standard deviations of the work paths are 6 kcal/mol at $z = -15$ Å for the backward direction and 6.3 kcal/mol at $z = 15$ Å for the forward direction.

pulling speeds, are the slopes from linear fittings to work profiles carried over 6 Å long trajectories in the z-direction. These slopes reflect the average work performed by pulling the proton along a distance of 1 Å in the z-direction. The first and second rows correspond to positive and negative pulling velocities, respectively. The Second Law of Thermodynamics is obeyed at all velocities. With decreasing speed the dissipated work decreases and the average work converges to the true free energy difference. Reversing the sign of the average work values in one of the rows and averaging over both pulling directions, the dissipative energy roughly cancels at all pulling speeds in support of our hypothesis. The free energy barrier for this test system depends only on internal energy, so the observed behavior may vary for systems with entropic barriers.

RESULTS AND DISCUSSION

The PMF for the proton permeation along the GlpF channel at 308 K, calculated by the method outlined in the previous section, is presented in Figure 4. Dashed and dotted lines correspond to the forward and backward profiles, respectively, and the solid line is their average shifted to equal zero at $z = -15$ Å. As expected, both the forward and backward profiles end higher than they began due to the dissipated energy. An upper bound to the deviation from the true profile can be estimated to be maximal at z = 15 Å for the forward profile and at $z = -15$ Å for the backward profile at around 6 kcal/mol for both cases. The deviation of the averaged profile from the true profile (for this model system) is likely to be significantly smaller because of a cancellation of dissipative energies. The exact matching between the averaged profile values at $z = -15$ Å and $z = 15$ Å is probably a coincidence yet is still reasonable since the proton is in nearby bulk water at both ends. We shall therefore discuss in the following para-

graph the features of the averaged PMF profile (solid line) assuming it is sufficiently converged.

In Figure 4 two major barriers are observed, one at the NPA motif at $z \approx 6$ Å and another at the selectivity filter at $z \approx -4$ Å. The higher barrier at the NPA motif is ~18.5 kcal/mol. The barrier at the selectivity filter is lower at ~11.5 kcal/mol, suggesting its main function may be in the steric exclusion of large solutes and ions, rather than excess protons explicitly.

The excess proton CEC was also constrained at various positions along the constriction region and the distribution of embedded water orientations was calculated; at each time step the pivot hydronium was identified with the MS-EVB2 state of maximum hydronium amplitude. Water molecules were observed to orient with their oxygen atoms pointing toward the pivot hydronium as would be expected from snapshots along a Grotthuss-type diffusion. This behavior was also observed from a short movie of one CEC pulling trajectory. The MS-EVB2 algorithm does not prohibit the excess proton from transporting, in principal, also via other mechanisms such as by diffusion as a hydronium ion. Thus when forced through the channel the proton hops without displacing water molecules, such that the bidirectional orientation of the water-file is centered around the excess proton rather than around the water molecule at the NPA motifs. The Grotthuss-like mechanism of induced proton transport in GlpF results in a smooth PMF of PT compared with that of glycerol transport.[29] An extended analysis of the specific electrostatic origins to the barriers of PT in aquaporins is underway, and a comparison shall be made with the conjectures regarding the relationship of proton conductance to hydrogen bonding patterns from earlier MD simulations.[26]

The activation energy for water transport in aquaporins is estimated[30] at ~5 kcal/mol, and therefore, according to our results, the proton conduction rate is smaller by at least 10 orders of magnitude than that of water conduction[11] (~1.1 H_2O/ns/monomer). The overall description of the process of proton conduction may be modeled by a Poisson-Nernst-Planck-type[31] theory. The actual transport in such an approach is likely to be lower than predicted by rate theory because it involves basically a Markovian diffusion process over the width of the barrier region. The barrier recrossing effects would affect the frictional corrections to rate theory and probably lower the rate by another 1–2 orders magnitude because the width of the barrier region is so large. In addition, at low proton concentrations, the channel-entrance probabilities are small and would further decrease the rate of proton conductance. Nevertheless, the free energy barrier calculated in the present communication provides the dominant factor in the reduction of the proton conduction to a rate many orders-of-magnitude below the water conduction rate in the GlpF channel.

To summarize, the major finding of this communication is that the overall free energy barrier to explicit PT in an aquaporin channel at 308K is ~18 kcal/mol. The barrier is maximal at the NPA motif.

NOTE ADDED IN PROOF

After the acceptance of this manuscript, we became aware of three very recent papers[32-34] devoted to the issue of proton exclusion by aquaporin channels. Various phenomenological computational descriptions are utilized by the authors of these papers to obtain their results. All of them emphasize the importance of the electrostatics of the channel environment in blocking the proton permeation. However, the actual sizes of the computed free energy barriers are rather mixed in these papers. For example, for aquaporin-1 a barrier of around 15 kcal/mole was calculated in one paper[33] using various electrostatic methods, while a significantly lower barrier of 6–7 kcal/mole was estimated for the same channel in a different paper[32] using a non-deterministic stochastic hopping algorithm for the proton transport. It is noteworthy that the latter barrier is only slightly higher (by 1–2 kcal/mole) than the experimentally measured activation free energy for gramicidin A in phospholipid bilayer,[35] which is considered to be a good channel for proton conduction. It is hoped that the approach taken in the present work will eventually help to clarify these and other issues regarding aquaporin proton permeation. That is, the method we have implemented involves the calculation of an explicit free energy barrier for proton permeation which, in turn, comes directly from deterministic molecular dynamics simulations using an underlying potential energy function (MS-EVB2) that explicitly contains the physics of proton transport and shuttling in aqueous protein environments.

REFERENCES

1. Kozono D, Yasui A, King LS, Agre P. Aquaporin water channels: atomic structure molecular dynamics meet clinical medicine. J Clin Invest 2002;109:1395–1399.
2. Preston GM, Carroll TP, Guggino WB, Agre P. Appearance of water channels in Xenopus oocytes expressing red cell CHIP28 protein. Science 1992;256:385–387.
3. Pohl P, Saparov AM, Borgnia MJ, Agre P. Highly selective water channel activity measured by voltage clamp: analysis of planar lipid bilayers reconstituted with purified AqpZ. Proc Natl Acad Sci USA 2001;98:9624–9629.
4. Tournaire-Roux C, Sutka M, Javot H, Gout E, Gerbeau P, Luu DT, Bligny R, Maurel C. Cytosolic pH regulates root water transport during anoxic stress through gating of aquaporins. Nature 2003;25: 393–397.
5. Decoursey TE. Voltage-gated proton channels and other proton transfer pathways. Physiol Rev 2003;83:475–579.
6. Agmon N. The Grotthuss mechanism. Chem Phys Lett 1995;244: 456–462.
7. Brewer ML, Schmitt UW, Voth GA. The formation and dynamics of proton wires in channel environments. Biophys J 2001;80:1691–1702.
8. Lynden-Bell RM, Rasaiah JC. Mobility and solvation of ions in channels. J Chem Phys 1996;105:9266–9280.
9. Fu D, Libson A, Miercke LJW, Weitzman C, Nollert P, Krucinski

J, Stroud RM. Structure of a glycerol-conducting channel and the basis for its selectivity. Science 2000;290:481–486.

10. de Groot BL, Grubmuller H. Water permeation across biological membranes: mechanism and dynamics of aquaporin-1 and GlpF. Science 2001;294:2353–2357.

11. Tajkhorshid E, Nollert P, Jensen MØ, Miercke LJW, O'Connell J, Stroud RM, Schulten K. Control of the selectivity of the aquaporin water channel family by global orientational tuning. Science 2002;296:525–530.

12. Schmitt UW, Voth GA. The computer simulation of proton transport in water. J Chem Phys 1999;111:9361–9381.

13. Day TJF, Soudackov AV , Ĉuma M, Schmitt UW, Voth GA. A second generation multistate empirical valence bond model for proton transport in aqueous systems. J Chem Phys 2002;117:5839–5849.

14. Schmitt UW, Voth GA. A multi-state empirical valence bond model for proton transport in water. J Phys Chem B 1998;102:5547–5551.

15. Ĉuma M, Schmitt UW, Voth GA. A multi-state empirical valence bond model for weak acid dissociation in aqueous solution. J Phys Chem A 2001;105:2814–2823.

16. Smondyrev M, Voth GA. Molecular dynamics simulation of proton transport through the influenza A virus M2 channel. Biophys J 2002;83:1987–1996.

17. Smondyrev M, Voth GA. Molecular dynamics simulation of proton transport near the surface of a phospholipid membrane. Biophys J 2002;82:1460–1468.

18. Wu Y, Voth GA. A computer simulation study of the hydrated proton in a synthetic proton Channel. Biophys J 2003;85:864–875.

19. Marx D, Tuckerman ME, Hutter J, Parrinello M. The nature of the hydrated excess proton in water. Nature 1999;397:601–604.

20. Jarzynski C. Equilibrium free energy differences from nonequilibrium measurements: a master equation approach. Phys Rev E 1997;56:5018–5035.

21. Jarzynski C. Nonequilibrium equality for free energy differences. Phys Rev Lett 1997;78:2690–2693.

22. Hummer G, Szabo A. Free energy reconstruction from nonequilibrium single-molecule pulling experiments. Proc Natl Acad Sci USA 2001;98:3658–3661.

23. Smith W, Forester TR. The DL_POLY Molecular Simulation Package. CCLRC, Daresbury Laboratory, Daresbury, Warrington, England.

24. Cornell WD, Cieplak P, Bayly CI, Gould IR, Merz KM Jr, Ferguson DM, Spellmeyer DC, Fox T, Caldwell JW, Kollman PA. A second generation force field for the simulation of proteins, nucleic acids, and organic molecules. J Am Chem Soc 1995;117:5179–5197.

25. Jorgensen WL, Chandrasekhar J, Madura JD, Impey RW, Klein ML. Comparison of simple potential functions for simulating liquid water. J Chem Phys 1983;79:926–935.

26. Jensen MØ, Tajkhorshid E, Schulten K. Electrostatic tuning of permeation and selectivity in aquaporin water channels. Biophys J 2003;85:2884–2899.

27. Park S, Khalili-Araghi F, Tajkhorshid E, Schulten K. Free energy calculation from steered molecular dynamics simulations using Jarzynski's equality. J Chem Phys 2003;199:3559–3566.

28. Hummer G. Fast-growth thermodynamic integration: error and efficiency analysis. J Chem Phys 2001;114:7330–7337.

29. Jensen MØ, Park S, Tajkhorshid E, Schulten K. Energetics of glycerol conduction through aquaglyceroporin GlpF. Proc Natl Acad Sci USA 2002;99:6731–6736.

30. Agre P, Kozono D. Aquaporin water channels: molecular mechanisms for human diseases. FEBS Lett 2003;555:72–78.

31. Mamonov AB, Coalson RD, Nitzan A, Kurnikova MG. The role of the dielectric barrier in narrow biological channels: a novel composite approach to modeling single-channel currents. Biophys J 2003;84:3646–3661.

32. de Groot BL, Frigato T, Helms V, Grubmueller H. The mechanism of proton exclusion in the aquaporin-1 water channel. J Mol Biol 2003;333:279–293.

33. Burykin A, Warshel A. What really prevents proton transport through aquaporin? Charge self-energy versus proton wire proposals. Biophys J 2003;85:3696–3706.

34. Chakrabarti N, Tajkhorshid E, Roux B, Pomes R. Molecular basis of proton blockage in aquaporins. Structure 2004;12:1–20.

35. Chernyshev A, Cukierman S. Thermodynamic view of activation energies of proton transfer in various gramicidin A channels. Biophys J 2002;82:182–192.